Integration of Machine Learning with Neutron Scattering for the Hamiltonian Tuning of Spin Ice under Pressure

A. M. Samarakoon,[1,2,3] D. Alan Tennant,[1,2] Feng Ye,[1] Qiang Zhang,[1] and S. A. Grigera[4]

[1]*Neutron Sciences Division, Oak Ridge National Laboratory, Oak Ridge, TN 37831, USA.*
[2]*Shull Wollan Center - A Joint Institute for Neutron Sciences, Oak Ridge National Laboratory, TN 37831. USA*
[3]*Materials Science Division, Argonne National Laboratory, Argonne, IL, USA*
[4]*Instituto de Física de Líquidos y Sistemas Biológicos, UNLP-CONICET, La Plata, Argentina*

This file includes information on :

1. $Dy_2Ti_2O_7$ crystal and pressure cell
2. Formulation of the optimal region
3. Quantitative predictions of the generative model
4. Temperature dependence of ambient pressure solution
5. Methods to constrain the value of J_1
6. Additional numerical studies as a function of J_3'

Supplementary note 1. $DY_2TI_2O_7$CRYSTAL AND PRESSURE CELL

As shown in Supplementary Figure 1(a), a cylindrical single-crystal (SL) of $Dy_2Ti_2O_7$was used for the pressure experiment. First, the sample was polished to fit the Teflon tube and glued to the Teflon cap. Next, the Teflon tube was filled with Fluorinert FC-770 as a pressure transmission medium before installing the crystal. Then, the sample is installed at room temperature, with care taken not to trap any air bubbles inside, and a Copper-beryllium cell was used to apply hydrostatic pressures, as shown in Supplementary Figure 1(b). The orientation of the single crystal was initially checked using x-ray Laue, cut as a prism using diamond and loaded into the clamp pressure cell. The orientation is further checked at low temperature. It is worth pointing out, however, that since the instrument is a white beam difractometer with large detector coverage, and we are interested in the magnetic diffuse signal, the crystal orientation is not critical for these measurements. Finally, the Cadmium was used to mask the cell portions except where the DTO crystal is present. The magnetic diffuse signal is in the low momentum transfer regime and not affected by the signal from the Teflon capsule.

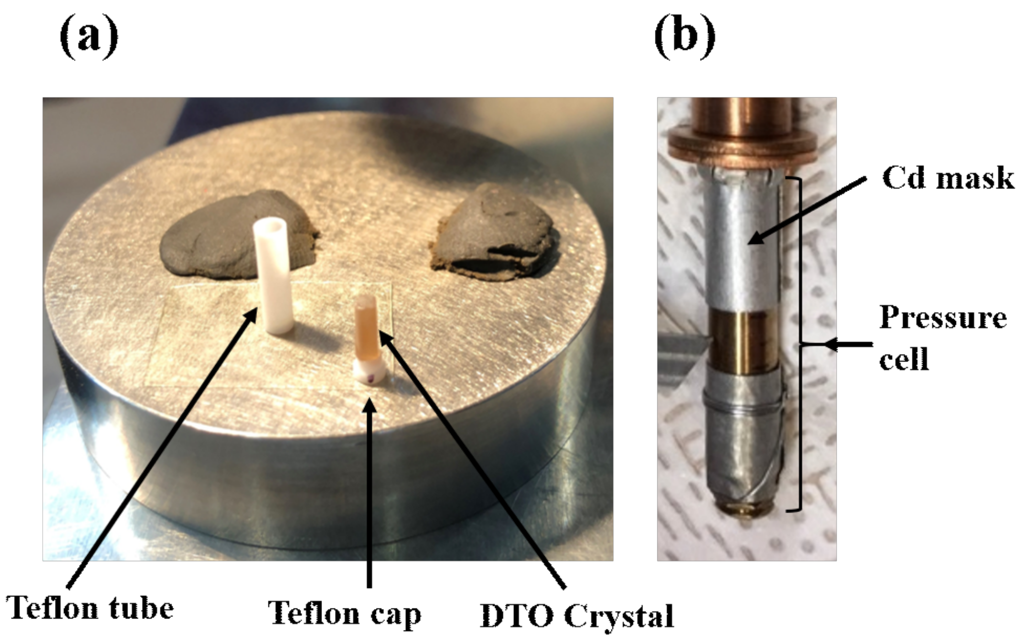

Supplementary Figure 1. **Pressure cell setup** (a) The Teflon tube and the polished Dy2Ti2O7 single-crystal attached to the Teflon cap. (b) The Copper-beryllium cell with a Cd mask covering outside the Teflon tube window.

Supplementary note 2. FORMULATION OF THE OPTIMAL REGION

The four-dimensional optimal region for which χ^2_{L} (0 G.Pa) $< C^2_{\mathrm{L}}$, as illustrated in Fig. 4 (blue contours), can be formulated by fitting the region to a minimum volume ellipsoid [1] as,

$$V \times M \times V^{\dagger} \leq 1$$

with

$$M = \begin{bmatrix} 4 & 7 & 10 & 25 \\ 7 & 1300 & 3910 & 1909 \\ 20 & 3910 & 11774 & 5829 \\ 25 & 1909 & 5828 & 6998 \end{bmatrix},$$

and

$$V = [J_1 - 3.336J_2 - 0.008J_3 + 0.019J_3' - 0.042].$$

For the minimum volume episode for the condition χ^2_{L} (1.3 G.Pa) $< C^2_{\mathrm{L}}$, as illustrated in Fig. 4 (red contours),

$$M = \begin{bmatrix} 4 & -16 & -47 & -31 \\ -16 & 1958 & 5858 & 2255 \\ -47 & 5858 & 17536 & 6752 \\ -31 & 2255 & 6752 & 5927 \end{bmatrix},$$

and

$$V = [J_1 - 3.446J_2 + 0.001J_3 + 0.016J_3' - 0.075].$$

The minimum volume episode for the condition χ^2_{multi} (0 G.Pa) $< C^2_{\mathrm{multi}}$, as illustrated in Fig. 4 (black contours),

$$M = \begin{bmatrix} 41 & -118 & -203 & -158 \\ -118 & 2601 & 7328 & 3612 \\ -203 & 7328 & 21226 & 10443 \\ -158 & 3612 & 10443 & 10180 \end{bmatrix},$$

and

$$V = [J_1 - 3.274J_2 + 0.114J_3 - 0.02J_3' - 0.045].$$

Supplementary note 3. QUANTITATIVE PREDICTIONS OF THE GENERATIVE MODEL

The generative model (GM) can directly calculate the latent space coordinates based on the microscopic parameters of the Hamiltonian, thus bypassing the computer-intensive Monte Carlo Simulations. Supplementary Figure 2 shows a quantitative comparison of the predictions from the GM compared with direct MC calculations.

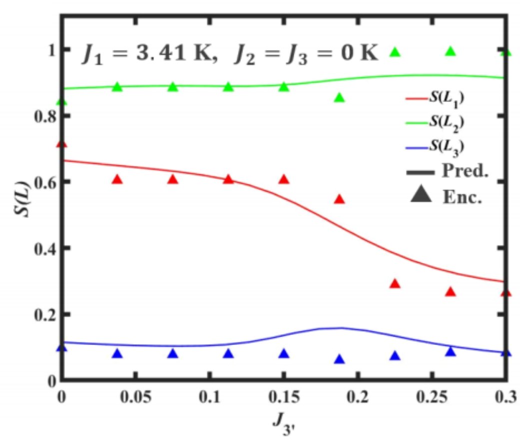

Supplementary Figure 2. **Generative model parameter predictions** Comparison between the latent space coordinates, S(L), for the simulated structure factor (filled triangles) and those predicted from the GM (solid lines) for an increasing value of the exchange parameter J_3'

Supplementary note 4. TEMPERATURE DEPENDENCE OF AMBIENT PRESSURE SOLUTION

The temperature dependence of $S(Q)$ for the 0 G.Pa. solution is shown in Supplementary Figure 3. Similar temperature dependence is shown in Fig. 5 in the main text for the solution at 1.3 GPa. Both solutions show diffuse scattering for Coulombic correlations associated with the isotropic U(1) gauge liquid at 1.5 K.

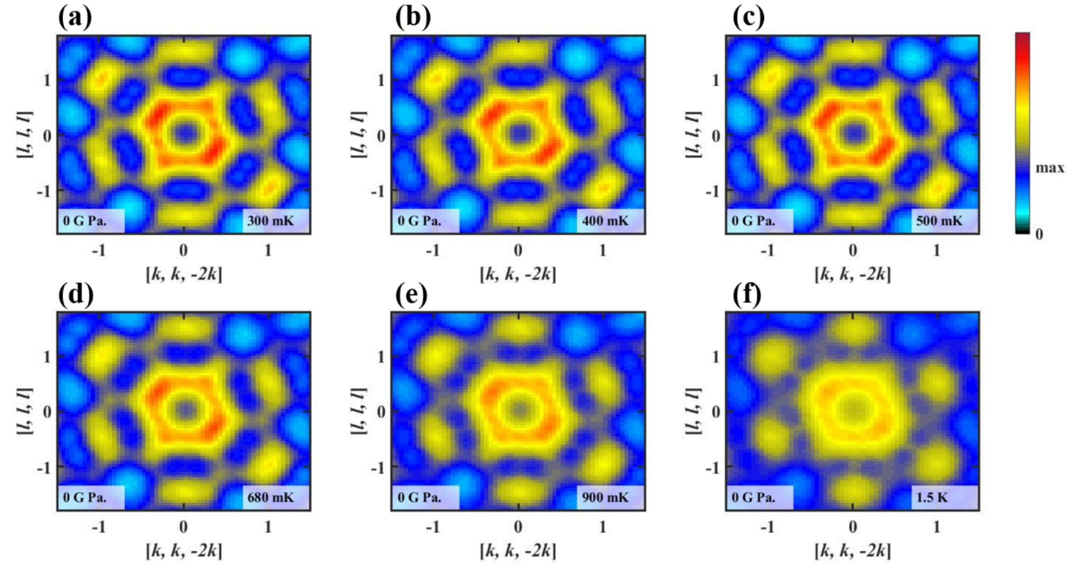

Supplementary Figure 3. **Temperature dependence of the simulated optimal structure factor.** The simulated structure factors for the optimal Hamiltonian parameters to the 680 mK ambient pressure data set at (a) 300 mK, (b) 400 mK, (c) 500 mK, (d) 680 mK, (e) 900 mK and (f) 1.5 K.

Supplementary note 5. METHODS TO CONSTRAIN THE VALUE OF J_1

The optimal region for just $S(Q)$ does not constrain J_1 and $J_2 - 0.335J_3 = 0.0144$ K. As shown in Supplementary Figure 4(a), the $S(Q)$ does not change as a function of J_1 at fixed $J_2 = 0.008$ K, $J_3 = -0.019$ K, $J_3' = 0.042$ K and $D = 1.3224$ K. The temperature dependence for each J_1 is also checked, and the $S(Q,T)$ is also not a good discriminator as summarized in Supplementary Figure 4 (c). However, the heat capacity provides a way to refine J_1 further, as demonstrated in Supplementary Figure 4(b), and Fig. 4. Only the heat capacity at ambient pressure is available.

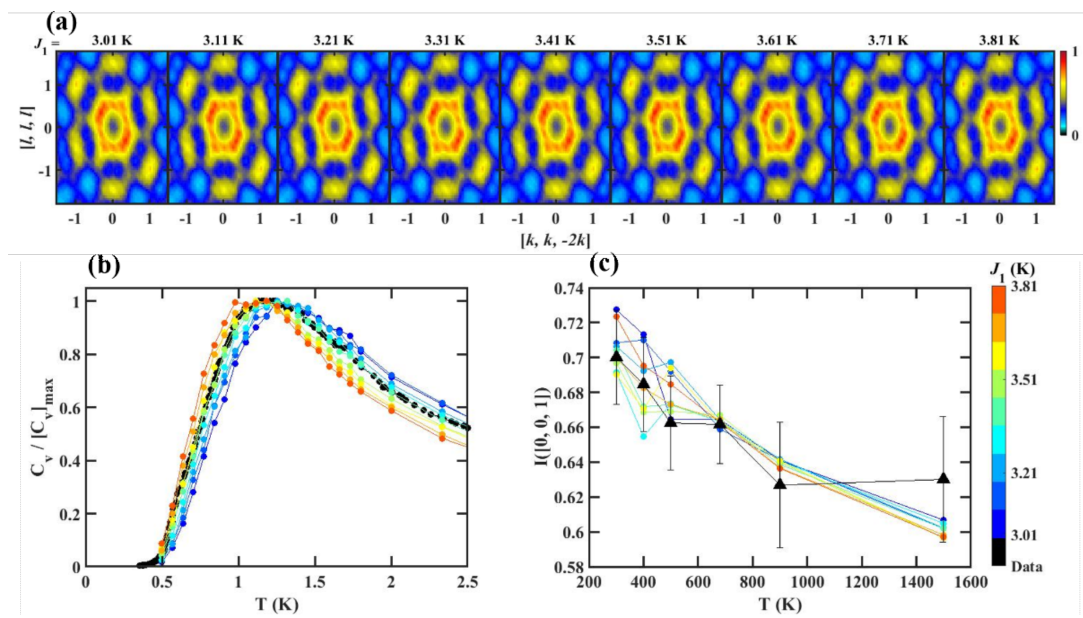

Supplementary Figure 4. **The effect of** J_1 **on some observable quantities.** (a) Structure factor and (b) heat capacity as a function of J_1 at fixed $J_2 = 0.008$ K, $J_3 = -0.019$ K, $J_3' = 0.042$ K and $D = 1.3224$ K. (c) the integrated intensity of the [0,0,1] diffuse peak as a function of temperature and J_1.

Supplementary note 6. ADDITIONAL NUMERICAL STUDIES AS A FUNCTION OF J_3'

Heat capacity, Zero-Field-Cooled (ZFC) and Field-Cooled (FC) susceptibilities were calculated for the same parameter sets used in Fig. 6. The heat capacity seems to evolve slightly with J_3' (Supplementary Figure 5 (a)). However, as discussed in the main text, the model crosses over from one diffuse phase to another, as evident by their correlations (see Fig. 6(d)). Even though the irreversibility temperature, $T_{\rm irr}$ does not any change with J_3', the susceptibility $\chi_{\rm DC}$ seems to have a different temperature dependence below $T_{\rm irr}$. This behavior may reflect the local structure of the magnetic phase deep into J_3' is different from the inter-twined ferromagnetic domain structure proposed in ref [2]. More numerical investigations are needed to learn the underlying physics of this phase.

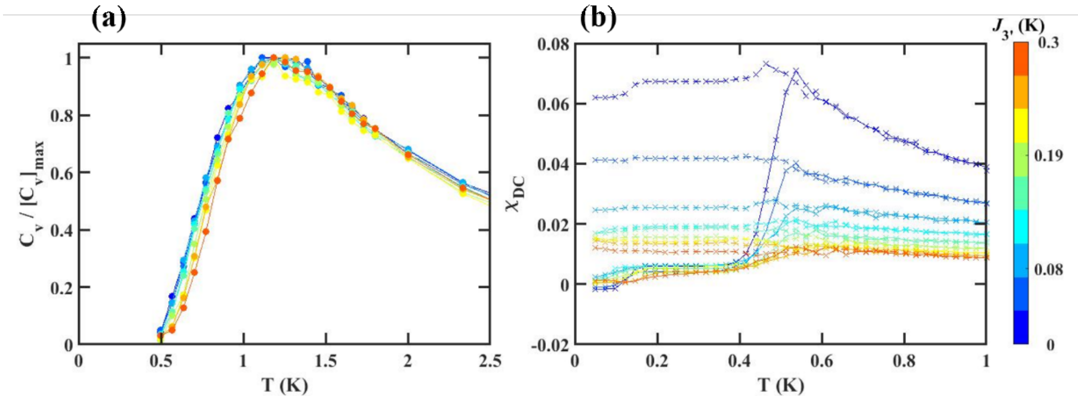

Supplementary Figure 5. **The effect of J_3' on some observable quantities.** (a) Simulated Heat capacity and (b) Zero-Field-Cooled (ZFC) and Field-Cooled (FC) susceptibility as a function of temperature by varying J_3' at $J_1 = 3.33$ K, $J_2 = -0.05$ K, $J_3 = 0$ K and $D = 1.3224$ K.

SUPPLEMENTARY REFERENCES

[1] N. Moshtagh *et al.*, Convex optimization **111**, 1 (2005).
[2] A. M. Samarakoon *et al.* Phys. Rev. Research 4, 033159 (2022).